Bioinformatics, 2026, **42**(2), btag042
https://doi.org/10.1093/bioinformatics/btag042
Published: 24 January 2026
Original Paper | Structural bioinformatics

OXFORD

GeoGAD: geometry-aware antibody design framework for complementarity-determining region precision engineering

Songjian Wei[1], Jinxiong Zhang[1,2,*], Yan Chen[1,2], Chunyan Tang[1,2], Jiayang Tan[1]

[1]School of Computer, Electronics and Information, Guangxi University, Nanning, Guangxi 530004, China
[2]Key Laboratory of Parallel Distributed and Intelligent Computing in Guangxi Universities and Colleges, Guangxi Center of Technology Innovation for Intelligent Digital Services, Nanning, Guangxi 530004, China
*Corresponding author. School of Computer, Electronics and Information, Guangxi University, 100 Daxue East Road,Nanning, Guangxi 530004, China. E-mail: zhangjx@gxu.edu.cn
Associate Editor: Arne Elofsson

Abstract

Motivation: **Antibodies, as pivotal effector molecules of the immune system, neutralize pathogens through specific binding to antigens mediated by complementarity-determining regions (CDRs), highlighting the critical importance of precise antibody design in diagnostics and therapeutics. Despite significant advances in CDR design, current methods remain limited by inadequate modeling of geometric constraints, omission of multi-scale spatial relationships, and insufficient conformational representation capacity—factors that collectively degrade prediction accuracy.**

Results: **To overcome these limitations, we present GeoGAD, a geometry-aware antibody design framework with Gaussian attention mechanisms. Key innovations include: (1) the introduction of rotational positional encoding to enhance geometric sensitivity; (2) a geometry-aware module that integrates multi-scale spatial features through dynamic message passing, adaptive edge refinement, and multi-edge-type coordinate optimization; and (3) a Gaussian attention mechanism that employs an edge-type-sensitive spatial Gaussian kernel to model long-range sequence dependencies, enabling focused attention on local critical residues while preserving global contextual modeling. Experimental evaluations demonstrate that GeoGAD achieves superior or comparable performance to state-of-the-art models across antibody sequence–structure co-modeling, CDR design, and affinity optimization benchmarks, particularly excelling in amino acid recovery rates (AAR) and structural accuracy metrics (RMSD, TM-score). By enhancing the design precision of antibody CDR regions, GeoGAD offers a geometrically consistent framework for the computational design of therapeutic antibodies.**

Availability and implementation: **The source code and implementation are available at https://github.com/WeiSongJian/GeoGAD, and the archival version for this manuscript is deposited at https://doi.org/10.5281/zenodo.18073443.**

1 Introduction

The primary goal of antibody design is the generation of therapeutic antibodies that bind target antigens with high affinity and specificity, thereby enabling effective neutralization or modulation of pathogens, cancer cells, or aberrant proteins. (Meganck and Baric 2021). This capability holds substantial promise for applications in infectious disease control, cancer immunotherapy, and autoimmune disorder intervention. In natural antibodies, precise recognition of antigenic epitopes is mediated by the complementarity-determining regions (CDRs) within the variable domains. Among the six CDRs, the heavy-chain CDR-H3 exhibits exceptional sequence and structural diversity and is widely regarded as the principal determinant of antigen-binding specificity (Maynard and Georgiou 2000, Akbar *et al.* 2021). Consequently, the accurate co-design of CDR-H3 sequence and three-dimensional conformation represents a central challenge in computational antibody engineering.

Antibodies are immunoglobulins utilized by the immune system to recognize and neutralize antigens (e.g., pathogens) (Murphy and Weaver 2016). Structurally, antibodies comprise two pairs of polypeptide chains—light and heavy chains—linked by disulfide bonds to form a characteristic Y-shaped architecture (Lu *et al.* 2020), as schematically depicted in Fig. 1. Each chain contains variable domains (VH for heavy chain; VL for light chain) followed by constant regions, with the variable regions organized into four framework regions (FRs) providing structural scaffolding and three CDRs (CDR-H1, CDR-H2, CDR-H3) responsible for antigen recognition.

Received: 23 October 2025. **Revised:** 31 December 2025. **Accepted:** 7 January 2026

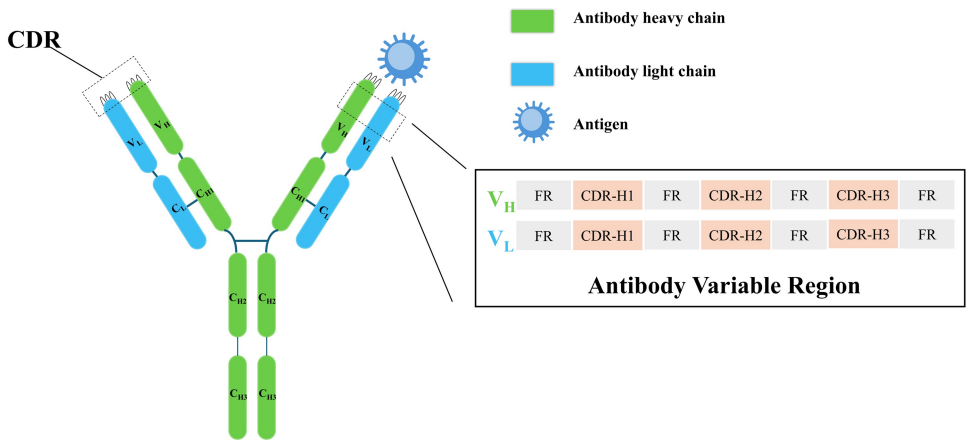

Figure 1 Schematic representation of antibody-antigen complex structure. Antibodies are Y-shaped heterotetrameric proteins comprising two identical heavy chains and two identical light chains.

Fundamentally, antibody design constitutes a specialized form of function-driven protein engineering. When constrained to fixed backbone architectures, global sequence optimization based on conditional probability distributions remains a central challenge in protein design (Xiong *et al.* 2020, Chu *et al.* 2024). In a broader protein design context, several approaches have sought to bridge this gap. DenseCPD (Qi and Zhang 2020) predicted amino acid probabilities for each residue by modeling the 3D density distribution of backbone atoms. ProDESIGN-LE (Huang *et al.* 2023) iteratively refined residue compatibility by learning geometric-chemical features within a Transformer framework. ProteinMPNN (Dauparas *et al.* 2022) implemented autoregressive sequence generation via masked self-attention mechanisms on topological backbone features. RFdiffusion (Watson *et al.* 2023) generated protein structures via a reverse denoising process grounded in diffusion model principles. These methods establish residue-structure correlations through geometric topological feature extraction, enabling deep learning-driven design. Sequence-based methods offer the advantage of leveraging abundant sequence data, which mitigates attribution biases from structural feature engineering (Sinai *et al.* 2017) and enables direct sequence-function mapping. Transformer language models such as ESM-1b (Rives *et al.* 2021) and ProGen (Madani *et al.* 2023) demonstrate sequence-to-function inference capabilities through unsupervised learning of residue dependencies in large-scale datasets. However, these kinds of models encounter functional-structural decoupling challenges: generated sequences may lack explicit structural constraints, resulting in unstable folds or infeasible conformations (Jeon and Kim 2024).

Conventional antibody engineering techniques, including hybridoma-based monoclonal antibody production and phage display selection, rely on experimental screening and iterative optimization. These methods are not only time- and labor-intensive but also constrained by the combinatorial complexity of the antibody sequence-structure space. While computational methodologies such as homology modeling and molecular docking have partially mitigated these challenges, they remain limited in modeling highly variable regions like CDRs and capturing essential binding conformations for antigen recognition.

Recent advances in deep learning have transformed computational antibody design through data-driven exploration of sequence-structure-function relationships. Structure-based generation approaches (e.g., ABlooper [Abanades *et al.* 2022], Ig-VAE [Eguchi *et al.* 2022]) concentrate on CDRs modeling by predicting backbone atomic 3D coordinates. However, these methods exhibit critical limitations in globally co-optimized structural and functional properties. Their reliance on local conformational sampling fails to capture framework (FRs) and antigen epitopes, and they cannot concurrently optimize sequence affinity and developability.(Cheng *et al.* 2024) Transformer-based antibody language models (AntiBERTy [Ruffolo *et al.* 2021], AbLang [Olsen *et al.* 2022], IgLM [Shuai *et al.* 2023]) enable end-to-end sequence generation from epitopes, overcoming limitations of inverse folding. Nevertheless, such sequence-only frameworks fail to explicitly encode 3D geometric information, resulting in questionable foldability of the generated antibody sequences (Gallo 2024). E (3)-equivariant graph neural networks, deep generative models, and diffusion-based frameworks—have transformed computational antibody design through data-driven exploration of sequence-structure-function relationships. RefineGNN (Jin *et al.* 2022b) introduced co-design of sequences and 3D structures using geometric graph representations. Subsequent models HSRN (Jin *et al.* 2022a) further enhanced the accuracy and efficiency of antibody design and docking by integrating hierarchical equivariant modeling and iterative structural optimization. DiffAb (Luo *et al.* 2022) employed denoising diffusion probabilistic models for CDR design. AbEgDiffuser (Zhu *et al.* 2025) integrated bilevel equivariant graph neural networks with evolutionary constraints to guide the diffusion-based generation of antibody CDRs. MEAN (Kong *et al.* 2023a) captured inter-chain spatial interactions via E (3)-equivariant message passing, and dyMEAN (Kong *et al.* 2023b) enabled end-to-end antibody generation through structure initialization and shadow paratope engineering. GeoAB (Lin *et al.* 2024) introduced geometric initializer and refiner units to generate CDRs with biophysically realistic internal geometries. ADesigner (Tan *et al.* 2024) implemented cross-gate MLP for antibody sequence-structure co-modeling. RAAD (Wu *et al.* 2025) incorporated multimodal features for relation-aware antibody design. Despite these advances, three fundamental limitations remain. (i) Insufficient geometric sensitivity hinders accurate modeling. Antibody function critically depends on precise alignment between secondary structural elements (β-sheets, α-helices) and 3D

spatial topology (Lin *et al.* 2024). However, conventional static positional encodings (Jin *et al.* 2022b; Kong *et al.* 2023a) fail to preserve SE(3)-equivariant representations during structural modeling, leading to physically infeasible predictions (Si and Yan 2024) that compromise stability. (ii) Geometric information decay occurs during long-sequence modeling. Previous work (Jeon and Kim 2024) demonstrates that geometric details degrade across message-passing layers, particularly in long CDR regions, preventing accurate structural reconstruction and impairing design precision. (iii) Inadequate multi-scale relationship integration limits model expressiveness. Antibody design requires simultaneous consideration of atomic-, residue-, and domain-level interactions, yet existing single-scale approaches (Luo *et al.* 2022, Kong *et al.* 2023b) neglect cross-scale dependencies that govern structural integrity.

To overcome these limitations, we propose GeoGAD (Geometry-aware Gaussian Attention-based Antibody Designer), a novel framework for structure-aware antibody design. GeoGAD incorporates rotary position embedding (RoPE) (Su *et al.* 2024) to capture relative sequential dependencies. Unlike absolute positional encodings, RoPE relies solely on topological indices, thereby addressing the SE(3)-equivariance preservation issue inherent in static representations. To simultaneously enhance geometric sensitivity and capture hierarchical geometric context, we introduce a geometry-aware module that fuses information across atomic, residue, and domain scales through dynamic message passing, adaptive edge feature updating, and multi-edge-type cooperative coordinate refinement. Additionally, we design an edge-type-sensitive Gaussian attention mechanism that leverages a spatial Gaussian kernel to concentrate attention on local critical residues while maintaining the capacity to model long-range dependencies—effectively mitigating geometric signal degradation in deep architectures. Taking both 1D sequences and 3D structures of antibody–antigen complexes as input, GeoGAD enables end-to-end joint generation of antibody sequences and conformations through the synergistic integration of geometric reasoning and Gaussian attention. Extensive experiments show that GeoGAD achieves state-of-the-art performance across three critical tasks: antibody sequence-structure co-modeling, CDR design, and affinity optimization, validating its effectiveness in addressing longstanding challenges in computational antibody design.

2 Materials and methods

2.1 Task formulation

An antibody-antigen complex A consists of L amino acid residues, with the i-th position residue defined as s_i, where $s_i \in \{\text{ACDEFGHIKLMNPQRSTVWY}\}$ and $i = 1, \ldots, L$. Here, different letters correspond to distinct amino acid types. Each amino acid s_i is characterized by the 3D coordinates of its four backbone atoms ω $(\omega \in \{C\alpha,\ N, C, O\})$. Let $x_{i,\omega} \in \mathbb{R}^{1\times 3}$ denote the coordinate of backbone atom ω of i-th position residue s_i, 3D structure of an amino acid residue s_i is characterized as a coordinate matrix $X_i \in \mathbb{R}^{4\times 3}$, namely $X_i = (x_{i,C_\alpha}^T, x_{i,N}^T, x_{i,C}^T, x_{i,O}^T)^T$. Given an antibody-antigen complex A, we define its CDRs as $AC = \{(s_i, X_i) | i = p, p+1, \ldots, p+q-1\}$, where p and q represent the starting position and length of CDRs, respectively. Antibody design aims to establish a deterministic mapping $F : A \rightarrow AC$. In this task, our proposed framework incorporates geometric information derived from antibody structural statistics to design CDRs with enhanced physical plausibility.

2.2 Overview

We propose a joint antibody sequence-structure co-design framework GeoGAD (Geometry-aware Gaussian Attention-based Antibody Designer), which receives 3D structural coordinates of antibody-antigen complexes and 1D sequences of antibody and antigen as dual-input, integrating multi-scale geometric constraints through progressive hierarchical modeling. The architecture of GeoGAD comprises three functional modules: (i) a geometric feature encoder that extracts sequence and structural features, (ii) a geometric-aware module with 4 layers of message-passing neural networks (MPNNs) incorporating Gaussian attention mechanisms for feature updating, and (iii) a collaborative decoder that simultaneously predicts categorical residue distributions and regresses 3D structural coordinates in a non-autoregressive manner. Fig. 2 presents the complete workflow.

2.3 Antibody-antigen complex heterogeneous graph representation and feature extraction

We formulate antibody-antigen complexes as heterogeneous graph $\mathcal{G} = (\mathcal{V}, \mathcal{E})$ with node set $\mathcal{V} = \mathcal{V}_H \cup \mathcal{V}_L \cup \mathcal{V}_A$, where $\mathcal{V}_H, \mathcal{V}_L, \mathcal{V}_A$ represent heavy chain, light chain, and antigen residues respectively. Each node $v_i \in \mathcal{V}$ is represented by a geometric feature vector h_i and a coordinate matrix $X_i \in \mathbb{R}^{4\times 3}$ encoding the 3D positions of its four backbone atoms (N, C_α, C, O). Following Lin *et al.* (Lin *et al.* 2024), the edge set $\mathcal{E}$ comprises 3 heterogeneous edge types defined by spatial proximity, sequential continuity, and residue-residue correlations which collectively characterize the structural dependencies between residues v_i and v_j. To aggregate global context features, we introduce 3 global nodes for heavy chain, light chain and antigen chain respectively. These global nodes are fully connected with each other and linked to all other nodes within their respective chains.

To enhance contextual feature representation for CDRs, we define the following three heterogeneous edge types in graph $\mathcal{G}$: (i) Intra-chain Context Edge, which captures local dependencies using geometric constraints. These are categorized as: Spatial proximity edges (connecting residues with C_α radial distance $\leq$8Å), Sequence adjacency edges (connecting residues with sequential offsets of ±1 and ±2), and K-nearest neighbor edges (connecting each residue to its 8 spatially closest neighbors). (ii) Global Edge, which facilitates structural information aggregation across chain components. These include Global-local edges (connecting each global node to all residue nodes within its corresponding chain) and Global-global edges (connecting global nodes of different chains). (iii) Antibody-Antigen Interface Edges, which model binding interface interactions between antibody and antigen chains. These are defined as: Radial interface edges (connecting residues between antibody and antigen chains with C_α radial distance $<$ 12Å), and k-nearest interface edges

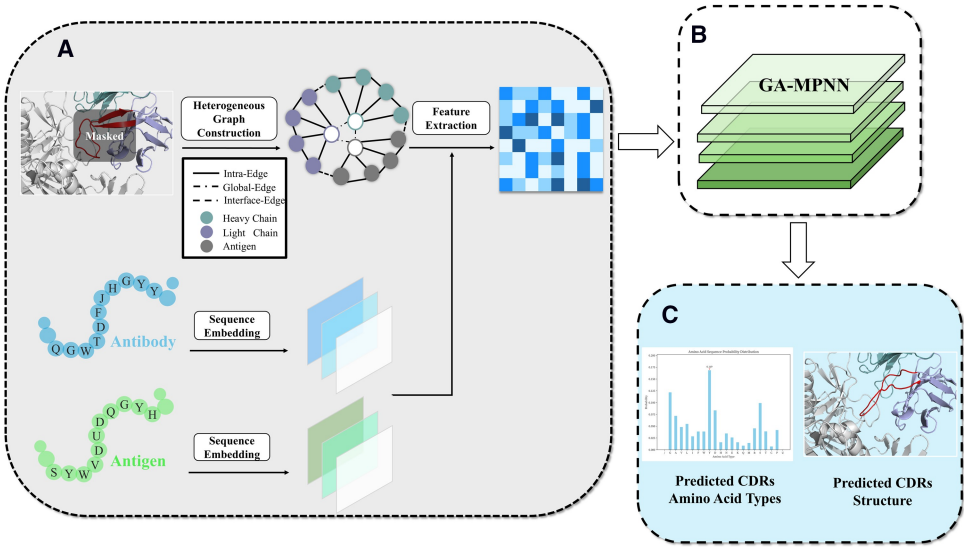

Figure 2 Schematic workflow of the Geometry-aware Gaussian Attention-based Antibody Designer (GeoGAD). The framework receives dual-modal inputs: antibody-antigen complex sequences and structures, with CDR-H3 regions masked using dedicated mask tokens. The pipeline of GeoGAD proceeds through three stages: (A) Geometric feature encoding. Antibody/antigen sequences are embedded into node features and fused with geometrically annotated heterogeneous graphs to construct initial representations. (B) Geometry-Aware Gaussian Attention-based Framework. The initial representations are iteratively updated through four layers of message-passing neural networks (MPNNs) incorporating Gaussian attention mechanisms. (C) Cooperative Decoding. Leveraging the refined features, the Cooperative decoder synchronously predicts the probability distribution over amino acid types and the atomic coordinates for the masked CDR-H3 region, to generate sequences and structures by sampling from these distributions.

(connecting each antibody residue to its $K=8$ nearest antigen neighbors). Specifically, for an edge e_{ij}, we construct a comprehensive edge feature vector $\mathcal{E}_{ij}$ by concatenating geometric and topological descriptors. $\mathcal{E}_{ij}$ is composed of: (i) a one-hot encoding vector h_{type} indicating the specific edge category; (ii) a relative positional embedding h_{pos} derived from the sinusoidal encoding of the sequential distance $p_i - p_j$; (iii) a distance feature vector h_{dist} consisting of Radial Basis Function (RBF) encoded Euclidean distances between the C_α atom of the target node v_j and the four backbone atoms (N, C_α, C, O) of the source node v_i; (iv) an orientation feature h_{angle} represented by 4-dimensional unit quaternions derived from the relative rotation matrix $R_{ij} = O_i^T O_j$ between the local reference frames of the two residues, and (v) a direction feature vector h_{dir} containing the geometric displacement vectors from the target node's C_α atom to the backbone atoms of the source node, projected into the target residue's local reference frame to ensure rotational invariance.

For given node v_i, its initial feature h_i is defined as:

$$h_i = h_i^{type} \oplus h_i^{pos} \oplus RBF\left(h_i^{dist}\right) \oplus h_i^{angle} \oplus h_i^{orient} \tag{1}$$

where h_i^{type} denotes the masked residue type embedding; h_i^{pos} is the Rotary Position Embedding (RoPE), computed from the local position index p_i of the residue within its polypeptide chain:

$$h_i^{pos}[2k] = \cos\left(p_i \theta_k\right) \tag{2}$$

$$h_i^{pos}[2k+1] = \sin\left(p_i \theta_k\right)$$

where $\theta_k = 10000^{-2k/16}$. This formulation effectively captures relative sequential dependencies via rotation in the feature space. Since the embedding relies exclusively on sequence indices independent of the global 3D coordinate system, it preserves the SE(3)-invariance of the overall node representation, ensuring consistency under 3D rigid transformations. Complementing this topological encoding, the explicit 3D geometric information is incorporated through invariant physical descriptors computed from the backbone structure: h_i^{dist} denotes the set of three backbone interatomic distances: $N - C_\alpha$, $C - C_\alpha$, and $O - C_\alpha$, which are mapped to continuous features via a radial basis function $RBF(\cdot)$; h_i^{angle} consists of sine and cosine projections of backbone dihedral angles (ψ, ω, φ) and bond angles (β, α, γ); To compute the orientation feature h_i^{orient}, we construct a local reference frame $O_i \in \mathbb{R}^{3\times3}$ for each residue. We define the x-axis unit vector along the C_α bond direction, and the z-axis as the normalized cross product of the $N - C_\alpha$ and $C_\alpha - C$ vector, with the y-axis determined by the right-hand rule. h_i^{orient} then represents the coordinates of the backbone atom displacement vectors projected into this local frame.

Building upon this heterogeneous graph representation, we develop a geometry-aware Gaussian attention framework to enable accurate joint sequence–structure design of antibody CDR regions.

2.4 Geometry-aware Gaussian attention antibody designer

We present a novel Geometry-aware Gaussian attention framework for antibody design, comprising a geometry-aware module (Fig. 3A) and a Gaussian attention module (Fig. 3B).

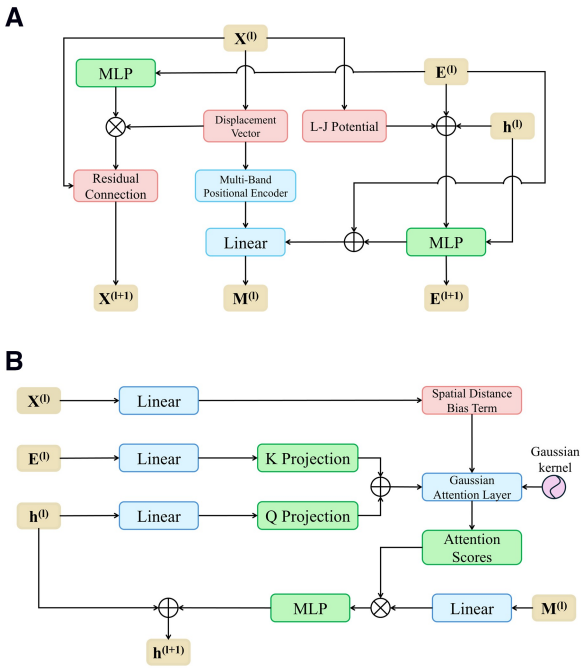

Figure 3 GeoGAD architecture. (A) Geometry-Aware Module: dynamically models antibody 3D structures by fusing multi-scale geometric features under physical constraints. The module comprises three components: Dynamic message passing with geometric priors, Adaptive edge feature updates, and Iterative coordinate refinement. This module integrates multi-band positional encoding and Lennard-Jones potential to enhance geometric awareness while ensuring physical plausibility. (B) Gaussian Attention Module: implements spatially accurate interaction modeling through edge-type-specific Gaussian kernels. The module operates in three stages: distance bias calculation using radial basis encoding functions (RBF), attention score generation, and context-aware node feature updating.

2.5 Geometry-aware module

The Geometry-Aware Module is designed to fuse multi-scale geometric context centered on individual residues. Specifically, the model encodes detailed geometric descriptors at the backbone atom level through high-dimensional embeddings, including interatomic relative positions, bond lengths, backbone dihedral angles, bond angles, and direction cosine vectors defined in a local reference frame. To capture diverse structural dependencies, the model employs heterogeneous edge types to explicitly represent sequential adjacency, spatial proximity, and intra- or inter-molecular interactions (e.g., within or between heavy chain, light chain, and antigen). Furthermore, to incorporate molecular-level context, global nodes are introduced for the heavy chain, light chain, and antigen, respectively, and chain-level information is aggregated via global–local attention or pooling mechanisms.

These multi-scale geometric signals are dynamically integrated through a multi-edge-type cooperative coordinate optimization mechanism. Each edge type is processed by a dedicated transformation network that produces scaling factors to differentially weigh the contributions of local geometric constraints, long-range spatial interactions, and molecular-entity guidance signals (see Equation (8)). This adaptive weighting enables unified modeling of local structural validity, inter-residue spatial compatibility, and global conformational consistency. The module operates in three sequential phases: (i) Dynamic geometric message passing, (ii) Adaptive edge feature updating, and (iii) Coordinate refinement.

Dynamic geometric message passing facilitates precise evolution of antibody 3D conformations via multi-layer geometric representation fusion and joint sequence-structure modeling. For residue pair (v_i, v_j) within local neighborhoods, we define the geometric features matrix $R_{ij} \in \mathbb{R}^{4\times4}$ to capture multi-channel spatial interactions. Specifically, let $\triangle X_{ij} \in \mathbb{R}^{4\times3}$ denote the coordinate difference matrix for the four backbone atoms between residues i and j. We compute the inner products of these difference vectors to generate the geometric Gram matrix $R_{ij} = \triangle X_{ij}\left(\triangle X_{ij}\right)^T$. These features are encoded into low-dimensional geometric descriptors through a differentiable mapping for efficient representation:

$$\tilde{\triangle} x_{ij} = f_\theta(vec(R_{ij})), f_\theta : \mathbb{R}^{16} \rightarrow \mathbb{R}^3 \tag{3}$$

where *vec* denotes the vectorization.

This mechanism captures statistical properties of spatial distributions by preserving second-order moment information (covariance matrices) to enforce robustness to structural variations. Inspired by Mildenhall *et al.* (2022), we propose a multi-frequency positional encoder to capture spatial relationships across scales. Specifically, we define a set of log-spaced frequency bases $\{\omega_k\}_{k=1}^K$, and for each residue pair (v_i, v_j), embed the relative displacement vector $\tilde{\triangle} x_{ij}$ into a multi-scale geometric representation by element-wise multiplication with each ω_k, followed by sine and cosine mappings:

$$\mathrm{P}_{ij}^{\sin} = \oplus_{k=1}^{K} \sin(\tilde{\triangle} x_{ij} \otimes \omega_k) \tag{4}$$

$$\mathrm{P}_{ij}^{\cos} = \oplus_{k=1}^{K} \cos(\tilde{\triangle} x_{ij} \otimes \omega_k)$$

where $\oplus$ denotes concatenation, $\otimes$ represents element-wise multiplication. The frequency parameters $\omega_k = 10^{-1+\frac{3(k-1)}{(K-1)}}$, are uniformly spaced on a logarithmic scale over the interval $[0.1, 100]$. This multi-frequency design enables the model to simultaneously capture fine-grained local geometry (via high-frequency components) and long-range spatial interactions (via low-frequency components), thereby mitigating geometric signal attenuation in deep network layers. Ablation studies (see Table 5) show that setting $K = 32$ yields the best trade-off between amino acid recovery rate (AAR) and structural accuracy (RMSD). Finally, the enhanced geometric features $P_{ij} = \left[P_{ij}^{\sin}, P_{ij}^{\cos}\right]$ are fed into the message generation network together with node features and edge-type encodings to drive geometry-aware message passing. For a given edge (v_i, v_j), the message vector m_{ij} is computed via fusion of three feature components:

$$m_{ij} = \phi_m\left(Concat\left(\psi\left(\left[h_i \| h_j\right]\right), \mathrm{P}_{ij}^{\sin} \oplus \mathrm{P}_{ij}^{\cos}, \mathcal{E}_{ij}\right)\right) \tag{5}$$

where ψ denotes MLP acting on the feature pair, $\mathcal{E}_{ij}$ represents edge features, and ϕ_m constitutes a four-layer message generation network.

Adaptive edge updating incorporates molecular dynamic priors by combining the Lennard-Jones potential (Lennard-Jones 1931) function with original edge features. Specifically, to capture van der Waals interactions, we explicitly calculate the potential V_{ij}^l based on the Euclidean distance r_{ij} between the C_α atoms of residue pairs:

$$V_{ij}^l = 4\mathcal{E}\left[\left(\frac{\sigma}{r_{ij}}\right)^{12} - \left(\frac{\sigma}{r_{ij}}\right)^{6}\right] \tag{6}$$

where $\mathcal{E}$ and σ are learnable parameters representing the potential depth and the zero-crossing distance, respectively. The calculated potential is then normalized to ensure numerical stability. The edge feature updating integrates three types of heterogeneous information, including node hidden states h_i^l and h_j^l, edge features $\mathcal{E}_{ij}^l$, and Lennard-Jones potential V_{ij}^l, and then applies the multilayer perceptron ϕ_e to perform feature updates:

$$\mathcal{E}_{ij}^{l+1} = \phi_e\left(h_i^l \oplus h_j^l \oplus \mathcal{E}_{ij}^l \oplus V_{ij}^l\right) \tag{7}$$

By integrating topological relationships and physical constraints into edge features, this design provides energy-guided optimization for coordinate refinement.

Coordinate updating employs multi-edge-type collaboration that enables adaptive modeling of geometric constraints via edge feature-based adaptive weighting. For node v_i, adjacent to k-th edge type, type-specific transformation network $\phi^{(k)}$ maps the edge feature $\mathcal{E}_{ij}^{(k)}$ to a scaling factor $s_{ij}^{(k)} = \phi^{(k)}\left(\mathcal{E}_{ij}^{(k)}\right)$, which is then broadcast across dimensions and element-wise multiplied with the coordinate difference vector $\Delta x_{ij}^{(k)}$ to generate the edge-type-sensitive geometric displacement vector $t_{ij}^{(k)} = \Delta x_{ij}^{(k)} \otimes s_{ij}^{(k)}$. Then an unordered segment-wise mean pooling strategy is exploited to integrate diverse edge type contributions. The final node coordinate update is formulated in a residual manner to enable iterative optimization, ensuring geometric plausibility of generated structures:

$$x_i^{(l+1)} = x_i^{(l)} + \frac{1}{|N(i)|}\sum_{k=1}^{K}\sum_{j \in N_k(i)} t_{ij}^{(k)} \tag{8}$$

where $x_i^{(l)}$ denotes the coordinate of node i at the l-th iteration layer, K represents the total number of edge types for node i, $N_k(i)$ denotes the neighborhood associated with the k-th edge type for node i, $N(i)$ represents the cardinality of the total neighborhood of node i, and $\phi_l^{(c)}$ is the edge-type-specific coordinate transformation network.

To further enhance the model's ability to jointly capture local critical interactions and long-range dependencies, we introduce a Gaussian attention mechanism built upon the geometry-aware module.

2.6 Gaussian attention module

The Gaussian attention mechanism enables precise modeling of critical residues in antibody structures through consideration of spatial distance constraints and feature similarity metrics. In essence, antibody-antigen interactions are a highly specific recognition process, where the free energy contribution of antigen epitopes binding to CDRs is significantly higher than that to intra-chain other intra-chain regions. The proposed geometric-aware Gaussian attention mechanism employs an edge-type-sensitive weighting strategy via adaptive Gaussian bias terms to enhance focus on critical information.

The spatial Gaussian kernel incorporates a covariance matrix-based Gaussian bias term to model local interaction patterns in antibody 3D structures. For node pairs (v_i, v_j) with edge type k, their geometric features are defined as:

$$\mathcal{G}_{ij} = exp\left(-\frac{\|x_i - x_j\|^2}{2\sigma^2}\right) \tag{9}$$

where σ denotes a learnable parameter that dynamically modulates the effective receptive field of the Gaussian kernel. The differentiable Gaussian kernel adaptively tunes the spatial receptive fields of distinct CDRs via backpropagation. It balances long-range structural coherence modeling with selective emphasis on local critical residues, thereby enhancing the discriminative capability for contextual structural patterns. Figure 4 presents the attention distribution heatmap of k-nearest neighbor edges and spatial sequential adjacency edges, using the heavy chain of antibody-antigen complex (PDB: 8dl6) as a case study. The results demonstrate preferential attention weights on local residues (e.g., adjacent or spatial neighbors), while non-local residue pairs with remote sequence distance also exhibit increased attention scores, confirming successful modeling of non-local spatial interactions. This observation validates the

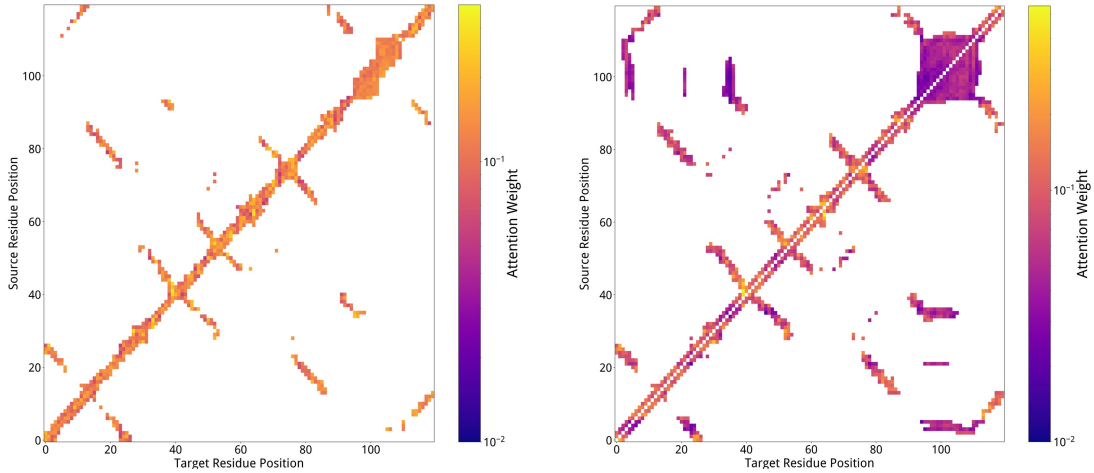

Figure 4 Visualization of edge attention distribution in antigen-antibody complex (PDB: 8dl6) heavy chain.

Gaussian attention mechanism's ability to harmonize local residue prioritization with global structural coherence.

The node dynamic feature updating is based on the orthogonal projection mechanism, aiming to enhance the synergistic expression capability between geometric features and sequence features. Attention scores are computed via bilinear projection:

$$\alpha_{ij}^{(k)} = Softmax_{\mathcal{N}_k(i)}\left(\left\langle W_Q h_i, W_K^{(k)} \tilde{h}_j^{(k)} \right\rangle + \mathcal{G}_{ij}^{(k)}\right) \tag{10}$$

where $W_K^{(k)}$ denotes the edge-type-specific projection matrix and $\tilde{h}_j^{(k)}$ is the flattened covariance matrix R_{ij} concatenated with node-feature $h_i^{(l)}$ and edge feature $e_{ij}^{(k)}$. After computing the Gaussian attention scores, messages from the k-th edge type, denoted $m_{ij}^{(k)}$, are aggregated using the corresponding attention weights as follows:

$$\tilde{m}_i = \sum_{k=1}^{K} \sum_{j \in N_k(i)} \alpha_{ij}^{(k)} \cdot m_{ij}^{(k)} \tag{11}$$

The aggregated message $\tilde{m}_i$ is then concatenated with the node feature $h_i^{(l)}$, transformed by a MLP, and added residually to produce the updated representation:

$$h_i^{(l+1)} = h_i^{(l)} + \psi\left(h_i^{(l)} \oplus \tilde{m}_i\right) \tag{12}$$

where ψ denotes the MLP.

2.7 Antigen-biding CDR-H3 co-decoding

Our framework enables end-to-end joint sequence-structure generation in a single forward pass via co-decoding, eliminating iterative refinement or autoregressive steps.

Sequence amino acid prediction outputs the probability distribution of amino acid types based on the updated node features $H \in \mathbb{R}^{N \times d_h}$:

$$p_\theta\left(s_i^{pred} | H_{masked}\right) = Softmax\left(W_s \cdot H_{masked}^{(i)} + b_s\right) \tag{13}$$

where $H_{masked}^{(i)}$ denotes the node features of the i-th masked residue, and W_s and b_s represent the classifier weight matrix and bias vector, respectively. This prediction mechanism relies solely on high-order node representations from the geometry-aware module without explicit concatenation of coordinate features, which reflects deep integration of sequence and structural information.

Atomic coordinate refinement is performed via residual updates for iterative optimization, where geometric displacement vectors for the four backbone atoms (N, C_α, C, O) of residue v_i are generated by the transformation network ϕ_ω:

$$\Delta\hat{x}_{i,\omega} = \phi_\omega\left(H_i^{(L)} \oplus \Gamma_{loc}\right) \quad \omega \in \{N, C_\alpha, C, O\} \tag{14}$$

$$\Delta Z_\omega^{(i)} = x_\omega^{(0)} + \Delta\hat{x}_{i,\omega}$$

where Γ_{loc} encodes relative position information of node coordinates according to Equation (7). This design introduces minimal perturbations at each update step through multi-scale geometric information fusion, thereby maintaining the physical plausibility of geometric constraints such as bond angles and dihedral angles.

2.8 Loss function

The loss function comprises three distinct components: sequence reconstruction loss, coordinate reconstruction loss, and contrastive loss.

The sequence reconstruction loss ($\mathcal{L}_{seq}$) is formulated as the cross-entropy criterion:

$$\mathcal{L}_{seq} = -\frac{1}{|\mathcal{M}|} \sum_{i \in \mathcal{M}} logp_\theta\left(s_i^{true} | H_{masked}, Z_{masked}\right) \tag{15}$$

where $\mathcal{M}$ denotes the set of masked amino acid positions and s_i^{true} represents the true residue type.

The coordinate reconstruction loss ($\mathcal{L}_{coord}$) is defined using the smooth L1 loss to quantify the deviation between predicted and ground-truth backbone atom coordinates:

$$\mathcal{L}_{coord} = \frac{1}{4|\mathcal{M}|}\sum_{i\in\mathcal{M}}\sum_{\omega}\ell_{smooth}\left(\|z_{i,\omega}^{pred} - z_{i,\omega}^{true}\|_2\right) \quad (16)$$

where $z_{i,\omega}^{pred}$ and $z_{i,\omega}^{true}$ denote the predicted and ground-truth coordinates, respectively, and ℓ_{smooth} ensures gradient smoothness.

In addition, we introduce a contrastive loss ($\mathcal{L}_P$) to encourage alignment between CDR and antigen epitope representations. For each antibody–antigen complex, we compute the mean residue embeddings over the CDR regions and the antigen epitope, respectively, and project them through a lightweight MLP head. The contrastive loss is then formulated as:

$$\mathcal{L}_{contrast} = -log\frac{exp\left(\phi\left(h_{CDR}, h_{ang}\right)/\tau\right)}{\sum_{k=1}^{K} exp\left(\phi\left(h_{CDR}, h_{ang}^{(k)}\right)/\tau\right)} \quad (17)$$

where h_{CDR} and h_{ang} represent the CDRs features and corresponding antigen epitope features, respectively, while negative samples $h_{ang}^{(k)}$ are sampled from other antigens within the same batch, with τ denoting the temperature coefficient.

The total loss function balances these three terms via a weighted summation:

$$\mathcal{L}_{total} = \mathcal{L}_{seq} + \alpha\mathcal{L}_{coord} + \beta\mathcal{L}_{contrast} \quad (18)$$

where α and β modulate the contributions of structural coordinate reconstruction and contrastive learning, respectively, and are optimized through validation set calibration.

3 Experiments

We adopt the experimental settings following prior works (Adolf-Bryfogle *et al.* 2018) and evaluate our model through three experimental scenarios: (i) Sequence-structure co-modeling on the Rosetta Antibody Design Database (Adolf-Bryfogle *et al.* 2018); (ii) Antigen-binding CDR-H3 design; (iii) Antibody affinity optimization.

3.1 Baselines

We compare against state-of-the-art antibody design methods as baselines, including: (i) LSTM-based antibody design approach (Saka *et al.* 2021), generating sequences in an autoregressive fashion; (ii) RefineGNN (Jin *et al.* 2022a), focusing on heavy chain modeling with autoregressive residue generation; (iii) C-RefineGNN (Kong *et al.* 2023a), extending RefineGNN to model the entire antibody-antigen complex; (iv) DiffAb (Luo *et al.* 2022), a diffusion probabilistic model for antibody structure design; (v) MEAN (Kong *et al.* 2023a), employing E(3)-equivariant message passing mechanism to capture interactions within antibody-antigen complexes; (vi) dyMEAN (Kong *et al.* 2023b), featuring an adaptive multi-channel equivariant encoder for full-atom geometric feature extraction; (vii) ADesigner (Tan *et al.* 2024), utilizing a cross-gated MLP for sequence-structure co-learning; (viii) RAAD (Wu *et al.* 2025), performing relation-aware antibody design in a single forward pass through comprehensive node/edge feature integration; and (ix) AbEgDiffuser (Zhu *et al.* 2025), integrating bilevel equivariant graph neural networks with evolutionary constraints for diffusion-based antibody codesign.

3.2 Metrics

For sequence-structure co-modeling on the antibody structure database, we quantify sequence recovery using amino acid recovery rate (AAR) coupled with C_α root mean square deviation (RMSD) to assess local conformational accuracy at the atomic level. In the antigen-binding CDR-H3 design task, we additionally employ TM-score (Zhang and Skolnick 2004, Xu and Zhang 2010) to evaluate global structural topology alignment of antibody-antigen complexes alongside AAR and RMSD metrics. For antibody affinity optimization, we utilize binding energy ($\Delta\Delta G$) as the primary metric, which assesses the model's capability in enhancing antibody affinity by quantifying thermodynamic changes in binding interactions.

3.3 Sequence and structure modeling

We evaluate the sequence-structure co-modeling capability of our framework on the Structured Antibody Database (SAbDab). The database comprises 9108 antibody structures (current through August 2024). After excluding entries lacking antigen structures, we clustered the remaining 3,127 antibody-antigen complexes using MMSeqs2 following Jin *et al.*'s (Jin *et al.* 2022a) protocol, grouping antibodies with >40% CDR sequence identity into the same cluster. This yielded 765, 1093, and 1659 clusters for CDR-H1, CDR-H2, and CDR-H3, respectively. To assess model performance, we partitioned the clustered dataset into training,

Table 1 Mean performance metrics of 10-fold cross-validation for CDR-H3 sequence-structure co-design on SAbDab.

Model	CDR-H1		CDR-H2		CDR-H3	
	AAR↑	C_α-RMSD↓	AAR↑	C_α-RMSD↓	AAR↑	C_α-RMSD↓
DiffAb	61.34	1.02	37.66	1.20	25.79	3.02
AbDiffuser	62.76	1.08	41.10	1.16	29.58	2.83
MEAN	58.29	0.98	41.15	0.95	36.38	2.21
dyMEAN	63.52	0.84	55.41	0.82	37.19	2.09
ADesigner	64.34	0.82	55.52	0.79	37.37	1.97
RAAD	<u>67.64</u>	<u>0.77</u>	<u>58.87</u>	<u>0.72</u>	<u>37.71</u>	<u>1.91</u>
GeoGAD	**68.31**	**0.72**	**61.00**	**0.69**	**37.88**	**1.82**

Bold numbers indicate the best performance in each category, and underlined values denote the second-best.

Table 2 Comparative performance of antigen-conditioned CDR-H3 Design on RAbD Dataset.

Model	AAR↑	TM-score↑	C_α-RMSD↓
RosettaAD	22.50	0.9435	5.52
RefineGNN	29.79	0.8308	7.55
C-RefineGNN	28.90	0.8317	7.21
HERN	32.83	0.9684	3.12
C-HERN	34.51	0.9734	2.79
AbEgDiffuser (t = 100)	28.97	0.9802	2.99
MEAN	36.77	0.9812	1.81
dyMEAN	39.14	0.9825	1.66
ADesigner	40.94	0.9850	1.55
RAAD	41.26	**0.9874**	1.46
GeoGAD	**41.62**	<u>0.9853</u>	**1.40**

Bold numbers indicate the best performance in each category, and underlined values denote the second-best.

test, and validation sets with an 8:1:1 ratio. The experiment employed 10-fold cross-validation, with results presented in Table 1. GeoGAD demonstrates superior performance across all CDR regions in the SAbDab benchmark. In terms of sequence recovery (AAR), GeoGAD achieves values of 68.31% for CDR-H1, 61.00% for CDR-H2, and 37.83% for CDR-H3, significantly outperforming all baseline models. GeoGAD also excels in structural accuracy (C_α-RMSD), reducing RMSD by 0.05 Å (CDR-H1), 0.03 Å (CDR-H2), and 0.08 Å (CDR-H3) relative to the second-best model. Crucially, regarding structural accuracy, GeoGAD consistently outperforms the leading baseline, RAAD, achieving reductions of 0.05 Å, 0.03 Å, and 0.09 Å across the CDR-H1, H2, and H3 regions, respectively. This improvement validates our geometry-aware design strategy. Unlike RAAD, which depends on learned edge relations to infer coordinates, GeoGAD explicitly integrates RoPE and biophysical constraints via the Lennard-Jones potential. These mechanisms enforce stricter geometric consistency and physical plausibility, enabling GeoGAD to recover precise

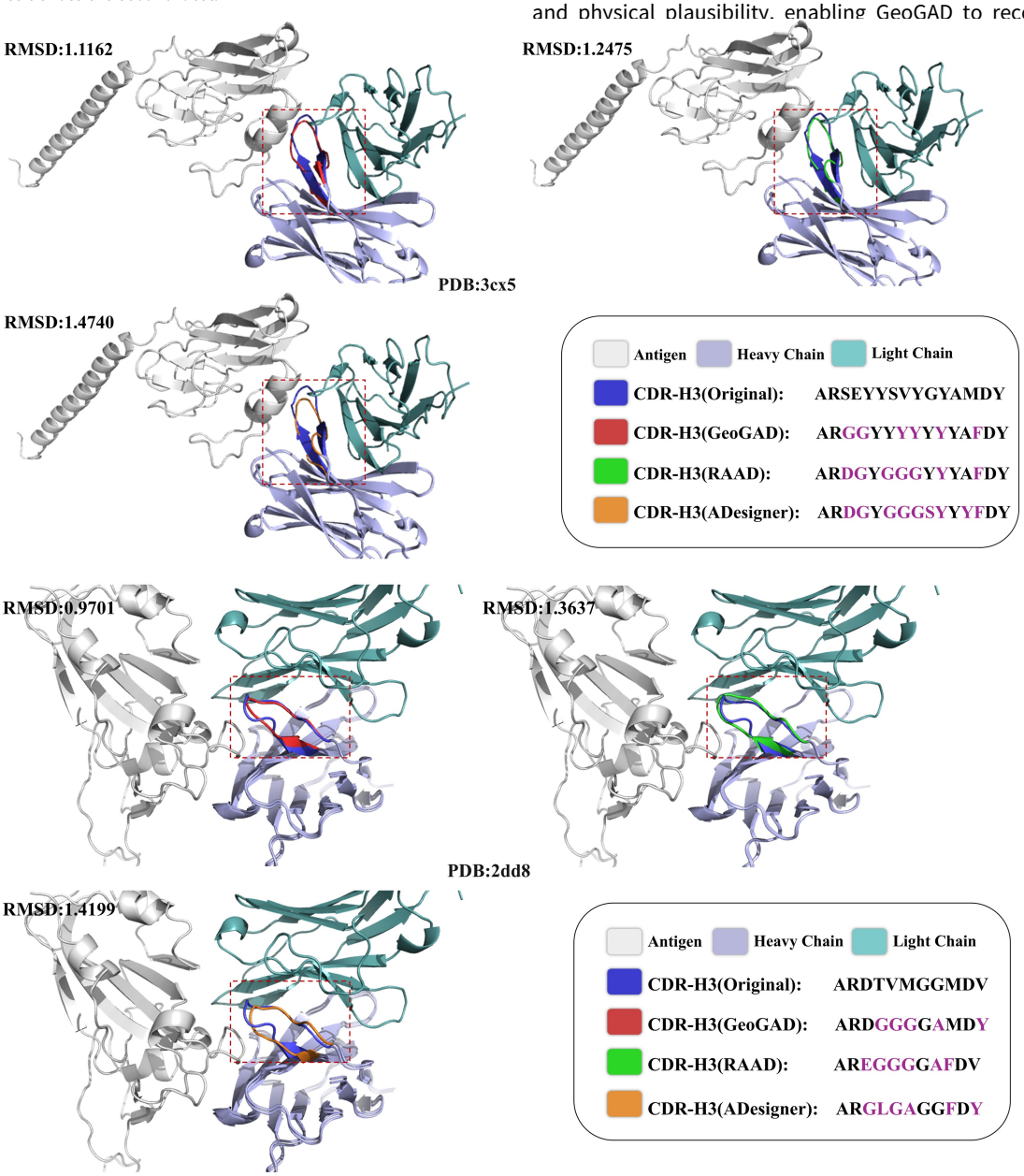

Figure 5 Comparative structural analysis of CDR-H3 regions for two antigen-antibody complexes (PDB: 2DD8, PDB: 3CX5). Generated structures from GeoGAD, RAAD, and ADesigner are superimposed with native structures, accompanied by corresponding RMSD metrics.

backbone conformations that pure relation-based approaches may miss.

3.4 Antigen-binding CDR-H3 design

We evaluate the model's capacity for generating antigen-binding CDR-H3 regions using the Rosetta Antibody Design (RAbD) dataset, which comprises 60 antigen-antibody complexes. The SAbDab dataset serves as the training set, excluding antibodies with CDR-H3 regions clustered identically to RAbD entries to prevent data leakage. The remaining data is partitioned into training and test sets at a 9:1 ratio. We include RosettaAD (Adolf-Bryfogle *et al.* 2018), a conventional benchmark method, for comparison alongside contemporary approaches. As shown in Table 2, our model achieves the highest AAR (41.62%) and the lowest Cα-RMSD (1.40 Å) among all evaluated methods. Although RAAD retains a marginal 0.21% lead in TM-score, GeoGAD surpasses it in structural accuracy with a 0.06 Å reduction in RMSD. This improvement highlights the model's capacity for fine-grained atomic refinement. The high AAR suggests that our multi-band positional encoding effectively captures the long-range sequence dependencies needed for accurate residue identification. Furthermore, the minimized RMSD confirms that Rotational Position Embeddings (RoPE) and Gaussian attention successfully enforce strict SE(3)-equivariant constraints, focusing the model on critical local interactions. Together, these components prioritize biophysical plausibility over broad topological approximations, rendering GeoGAD highly effective for therapeutic antibody design. Figure 5 presents comparative structural modeling of CDR-H3 regions for two randomly sampled antigen-antibody complexes (PDB: 2DD8 and PDB: 3CX5).

Table 3 Mean computed ΔΔG values following affinity optimization.

Model	△△G
Random	+1.52
LSTM	−1.48
RefineGNN	−3.98
C-RefineGNN	−3.79
MEAN	−5.33
dyMEAN	−7.31
ADesigner	−10.78
RAAD	−11.79
GeoGAD	−12.41

3.5 Antibody affinity optimization

Antibody affinity optimization represents a primary objective in therapeutic antibody design. To evaluate the model's performance in this task, we curated a test dataset comprising 53 high-quality antibody-antigen complex structures selected from the SKEMPI v2.0 database (Jankauskaitė *et al.* 2019). These complexes cover a diverse range of antigen types and binding interfaces, providing a robust benchmark for optimization. We evaluate △△G for optimized CDR-H3 sequences and structures. Following Kong et al.'s protocol (Kong *et al.* 2023a), binding energy predictions were performed using a geometric deep learning network (Shan *et al.* 2022). The iterative target enhancement algorithm (Yang *et al.* 2020) was employed as the optimization strategy. As presented in Table 3, our framework achieves state-of-the-art performance, with optimized CDR-H3 sequences and structures exhibiting significantly reduced △△G values, indicating enhanced binding affinity. Figure 6 visualizes the structural superposition between optimized and native conformations for two representative antibody-antigen complexes (PDB: 3LZF, optimized △△G: -14.077; PDB: 3SE9, optimized △△G: -12.401).

3.6 Ablation study

To systematically assess the contribution of each key component in GeoGAD, we perform ablation studies on two core tasks: Sequence and Structure Modeling and Antigen-Binding CDR-H3 Design. The ablation configurations are as follows: (i) replace rotary position encoding (RoPE) with standard sinusoidal positional encoding; (ii) remove the Lennard-Jones potential term, retaining only the base geometric edge features; (iii) disable the multi-band positional encoder during message updating; (iv) disabling of the Gaussian attention mechanism.

Table 4 demonstrates that, in the modeling task, ablating the Gaussian attention mechanism leads to a significant increase in RMSD, highlighting its critical role in recovering fine-grained local geometry. The removal of the multi-band positional encoder

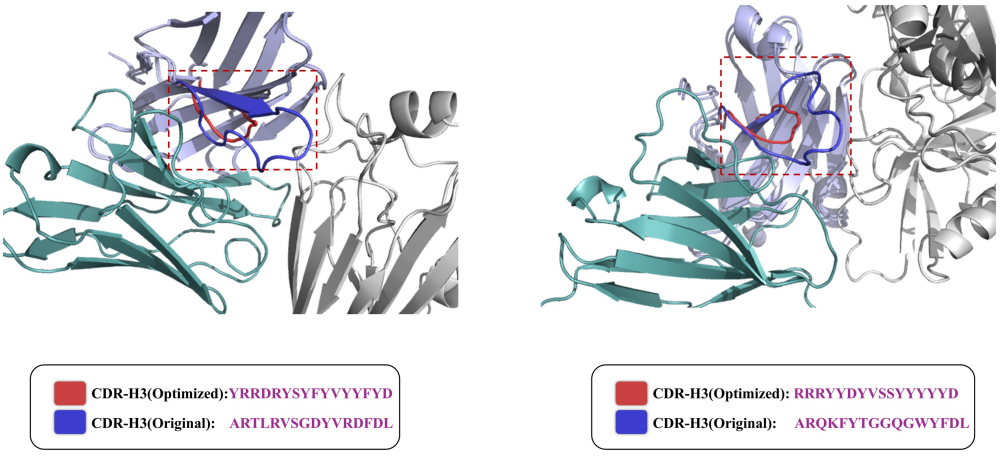

Figure 6 Structural superposition of affinity-optimized and native CDR-H3 regions for two representative antibody-antigen complexes.

Table 4 Component ablation analysis results.

	Modeling		Design		
	AAR↑	C_α-RMSD↓	AAR↑	TM-score↑	Cα-RMSD↓
GeoGAD	**37.83**	**1.83**	**41.62**	**0.9853**	**1.40**
w/o RoPE	37.10	1.89	38.17	0.9831	1.50
w/o Lennard-Jones potential	37.22	1.85	38.90	0.9848	1.48
w/o Multi-band positional encoder	36.79	1.85	39.86	0.9847	1.51
w/o Gaussian attention	36.63	1.95	35.92	0.9805	1.55

Bold numbers indicate the best performance in each category.

Table 5 Ablation study with varying numbers of frequency bands K.

	Modeling		Design		
K=	AAR↑	Cα-RMSD↓	AAR↑	TM-score↑	Cα-RMSD↓
8	36.55	1.90	39.66	0.9828	1.53
16	36.62	1.91	40.07	0.9821	1.43
32	**37.83**	**1.83**	**41.62**	**0.9853**	**1.40**
64	37.24	1.86	41.25	0.9833	1.51
128	36.47	1.91	40.94	0.9798	1.53

Experimental results show that $K = 32$ yields the highest amino acid recovery rate (AAR), the lowest RMSD, and the highest TM-score, demonstrating that this configuration achieves an optimal trade-off between model expressivity and generalization.
Bold numbers indicate the best performance in each category.

causes the largest drop in amino acid recovery rate (AAR), underscoring its effectiveness in capturing long-range sequential dependencies. In the design task, both the multi-band positional encoder and Gaussian attention are essential: their removal results in substantial degradation in both AAR and TM-score. Notably, while RoPE has minimal impact on modeling performance, its absence in the generation task leads to markedly worse TM-score and higher RMSD, confirming its importance for ensuring the physical validity of generated antibody structures. Finally, although the Lennard-Jones potential does not produce a dramatic performance gain, it consistently yields modest improvements across both tasks.

To systematically assess the influence of the number of frequency bands K in the multi-band positional encoding on model performance, we perform an ablation study over K. As defined in Equation (4), K governs the resolution of geometric signal representation in the multi-frequency space: a small K may fail to capture the full range of spatial relationships—from local bond angles to long-range spatial interactions—whereas an excessively large K risks introducing redundant frequency components. We therefore evaluate $K \in \{8, 16, 32, 64, 128\}$ on two core tasks, namely structure modeling and sequence design, with results reported in Table 5.

4 Conclusion

In this paper, we propose **Geo**metry-aware **G**aussian Attention-based **A**ntibody **D**esigner (GeoGAD), which demonstrates significant advantages in antibody sequence-structure co-design by incorporating rotational position encoding, multi-level geometric representation modules, and Gaussian attention mechanisms. Experimental results show GeoGAD outperforms or matches state-of-the-art baselines in core metrics, including sequence recovery rate (AAR) and structural accuracy (RMSD, TM-score). Limitations include: (i) Strong data dependency, where performance is constrained by available high-quality antibody-antigen complex structures; (ii) Need for wet-lab validation, as current evaluation relies exclusively on computational metrics.

Based on the research foundation and limitations, future research priorities can advance the following directions: (i) for the data dependency problem, integrating semi-supervised learning and adversarial generative strategies, and integrating large-scale unlabeled antibody sequences and limited high-precision structural data, to improve generalization ability in few-shot scenarios, reducing dependence on high-quality complex structures; (ii) expanding the framework's geometric modeling capability to antigen epitopes, to adapt to design requirements in practical applications, such as responding to antigen conformational changes caused by pathogen variation or broad-spectrum neutralizing antibody design; (iii) establishing a feedback mechanism combining computational simulation with wet experimental validation, such as combining high-throughput screening platforms to perform in vitro crystal structure analysis of candidate antibodies, forming a data-model-experiment iterative optimization system.

Although the current research is still limited to computational metric validation, the proposed geometric perception paradigm provides a modeling approach with physical constraints for the antibody engineering field, providing a new technical pathway for the development of therapeutic antibodies.

Acknowledgments

Supported by the high-performance computing platform of Guangxi University. We sincerely thank all anonymous reviewers for valuable suggestions.

Author contributions

Songjian Wei (Conceptualization [equal], Data curation [equal], Investigation [equal], Methodology [equal], Visualization [equal], Writing—original draft [equal], Writing—review & editing [equal]), Jinxiong Zhang (Conceptualization [equal], Formal analysis [equal], Methodology [equal], Supervision [equal], Writing—review & editing [equal]), Yan Chen (Conceptualization [equal], Formal analysis [equal], Funding acquisition [equal], Supervision [equal]), Chunyan Tang (Formal analysis [equal], Supervision [equal]), and Jiayang Tan (Data curation [equal], Investigation [equal], Visualization [equal])

Conflict of interest

The authors declare no conflicts of interest.

Funding

This work was supported by the Guangxi Key Research and Development Plan Project [AB24010031] and the National Natural Science Foundation of China [62362004 and 61962004].

References

Abanades B, Georges G, Bujotzek A *et al.* ABlooper: fast accurate antibody CDR loop structure prediction with accuracy estimation. *Bioinformatics* 2022;**38**:1877–80.

Adolf-Bryfogle J, Kalyuzhniy O, Kubitz M *et al.* RosettaAntibodyDesign (RAbD): a general framework for computational antibody design. *PLoS Comput Biol* 2018;**14**:e1006112.

Akbar R, Robert PA, Pavlović M *et al.* A compact vocabulary of paratope-epitope interactions enables predictability of antibody-antigen binding. *Cell Rep* 2021;**34**:108856.

Cheng J, Liang T, Xie XQ *et al.* A new era of antibody discovery: an in-depth review of AI-driven approaches. *Drug Discov Today* 2024;**29**:103984.

Chu AE, Lu T, Huang PS. Sparks of function by de novo protein design. *Nat Biotechnol* 2024;**42**:203–15.

Dauparas J, Anishchenko I, Bennett N *et al.* Robust deep learning–based protein sequence design using ProteinMPNN. *Science* 2022;**378**:49–56.

Eguchi RR, Choe CA, Huang PS. Ig-VAE: generative modeling of protein structure by direct 3D coordinate generation. *PLoS Comput Biol* 2022;**18**:e1010271.

Gallo E. The rise of big data: deep sequencing-driven computational methods are transforming the landscape of synthetic antibody design. *J Biomed Sci* 2024;**31**:29.

Huang B, Fan T, Wang K *et al.* Accurate and efficient protein sequence design through learning concise local environment of residues. *Bioinformatics* 2023;**39**:btad122.

Jankauskaitė J, Jiménez-García B, Dapkūnas J *et al.* SKEMPI 2.0: an updated benchmark of changes in protein–protein binding energy, kinetics and thermodynamics upon mutation. *Bioinformatics* 2019;**35**:462–9.

Jeon W, Kim D. AbFlex: designing antibody complementarity determining regions with flexible CDR definition. *Bioinformatics* 2024;**40**:btae122.

Jin W, Barzilay R, Jaakkola T. Antibody-Antigen docking and design via hierarchical structure refinement. In *International Conference on Machine Learning*. PMLR, 2022a, 10217–10227.

Jin W, Wohlwend J, Barzilay R *et al.* Iterative refinement graph neural network for antibody sequence-structure co-design. arXiv, https://doi.org/10.48550/arXiv.2110.04624, 2022b, preprint: not peer reviewed.

Kong X, Huang W, Liu Y. Conditional antibody design as 3D equivariant graph translation. arXiv, https://doi.org/10.48550/arXiv.2208.06073, 2023a, preprint: not peer reviewed.

Kong X, Huang W, Liu Y. End-to-end full-atom antibody design. arXiv, https://doi.org/10.48550/arXiv.2302.00203, 2023b, preprint: not peer reviewed.

Lennard-Jones JE. Cohesion. *Proc Phys Soc* 1931;**43**:461–82.

Lin H, Wu L, Huang Y *et al.* GeoAB: towards realistic antibody design and reliable affinity maturation. bioRxiv, https://doi.org/10.1101/2024.05.15.594274, 2024, preprint: not peer reviewed.

Lu RM, Hwang YC, Liu IJ *et al.* Development of therapeutic antibodies for the treatment of diseases. *J Biomed Sci* 2020;**27**:1.

Luo S, Su Y, Peng X *et al.* Antigen-specific antibody design and optimization with diffusion-based generative models for protein structures. *Adv Neural Inf Process Syst* 2022;**35**:9754–67.

Madani A, Krause B, Greene ER *et al.* Large language models generate functional protein sequences across diverse families. *Nat Biotechnol* 2023;**41**:1099–106.

Maynard J, Georgiou G. Antibody engineering. *Annu Rev Biomed Eng* 2000;**2**:339–76.

Meganck RM, Baric RS. Developing therapeutic approaches for twenty-first-century emerging infectious viral diseases. *Nat Med* 2021;**27**:401–10.

Mildenhall B, Srinivasan PP, Tancik M *et al.* NeRF: representing scenes as neural radiance fields for view synthesis. *Commun ACM* 2022;**65**:99–106.

Murphy K, Weaver C. 2016. Janeway's immunobiology. Garland Science.

Olsen TH, Moal IH, Deane CM. AbLang: an antibody language model for completing antibody sequences. *Bioinform Adv* 2022;**2**:vbac046.

Qi Y, Zhang JZH. DenseCPD: improving the accuracy of neural-network-based computational protein sequence design with DenseNet. *J Chem Inf Model* 2020;**60**:1245–52.

Rives A, Meier J, Sercu T *et al.* Biological structure and function emerge from scaling unsupervised learning to 250 million protein sequences. *Proc Natl Acad Sci USA* 2021;**118**:e2016239118.

Ruffolo JA, Gray JJ, Sulam J *et al.* Deciphering antibody affinity maturation with language models and weakly supervised learning. arXiv, https://doi.org/10.48550/arXiv.2112.07782, 2021, preprint: not peer reviewed.

Saka K, Kakuzaki T, Metsugi S *et al.* Antibody design using LSTM based deep generative model from phage display library for affinity maturation. *Sci Rep* 2021;**11**:5852.

Shan S, Luo S, Yang Z *et al.* Deep learning guided optimization of human antibody against SARS-CoV-2 variants with broad neutralization. *Proc Natl Acad Sci USA* 2022;**119**:e2122954119.

Shuai RW, Ruffolo JA, Gray JJ. IgLM: infilling language modeling for antibody sequence design. *Cell Syst* 2023;**14**:979–89.e4.

Si Y, Yan C. Protein language model-embedded geometric graphs power inter-protein contact prediction. *Elife* 2024; **12**:RP92184.

Sinai S, Kelsic E, Church GM *et al.* Variational auto-encoding of protein sequences. arXiv, https://doi.org/10.48550/arXiv.1712.03346, 2017, preprint: not peer reviewed.

Su J, Ahmed M, Lu Y *et al.* RoFormer: enhanced transformer with rotary position embedding. *Neurocomputing (Amst)* 2024; **568**:127063.

Tan C, Gao Z, Wu L *et al.* Cross-gate MLP with protein complex invariant embedding is a One-Shot antibody designer. *AAAI* 2024;**38**:15222–30.

Watson JL, Juergens D, Bennett NR *et al.* De novo design of protein structure and function with RFdiffusion. *Nature* 2023; **620**:1089–100.

Wu L, Lin H, Huang Y *et al.* Relation-aware equivariant graph networks for epitope-unknown antibody design and specificity optimization. *In Proceedings of the AAAI Conference on Artificial Intelligence* 2025;**39**:895–904.

Xiong P, Hu X, Huang B *et al.* Increasing the efficiency and accuracy of the ABACUS protein sequence design method. *Bioinformatics* 2020;**36**:136–44.

Xu J, Zhang Y. How significant is a protein structure similarity with TM-score = 0.5? *Bioinformatics* 2010;**26**:889–95.

Yang K, Jin W, Swanson K *et al.* 2020. Improving molecular design by stochastic iterative target augmentation. In *International Conference on Machine Learning* PMLR, 10716–1072.

Zhang Y, Skolnick J. Scoring function for automated assessment of protein structure template quality. *Proteins: Structure, Function, and Bioinformatics* 2004;**57**:702–10.

Zhu Y, Shi X, Zhang J *et al.* AbEgDiffuser: antibody sequence-structure codesign with equivariant graph neural networks and diffusion models. *J Chem Theory Comput* 2025;**21**: 11307–17.

Bioinformatics, 2026, 42, 1–13
https://doi.org/10.1093/bioinformatics/btag042
Original Paper